

**Effect of dissolved KOH and NaCl on the solubility of water in hydrogen
A Monte Carlo simulation study**

Habibi, Parsa; Dey, Poulumi; Vlugt, Thijs J.H.; Moulτος, Othonas A.

DOI

[10.1063/5.0221004](https://doi.org/10.1063/5.0221004)

Publication date

2024

Document Version

Final published version

Published in

Journal of Chemical Physics

Citation (APA)

Habibi, P., Dey, P., Vlugt, T. J. H., & Moulτος, O. A. (2024). Effect of dissolved KOH and NaCl on the solubility of water in hydrogen: A Monte Carlo simulation study. *Journal of Chemical Physics*, 161(5), Article 054304. <https://doi.org/10.1063/5.0221004>

Important note

To cite this publication, please use the final published version (if applicable).
Please check the document version above.

Copyright

Other than for strictly personal use, it is not permitted to download, forward or distribute the text or part of it, without the consent of the author(s) and/or copyright holder(s), unless the work is under an open content license such as Creative Commons.






Takedown policy

Please contact us and provide details if you believe this document breaches copyrights.
We will remove access to the work immediately and investigate your claim.

RESEARCH ARTICLE | AUGUST 01 2024

Effect of dissolved KOH and NaCl on the solubility of water in hydrogen: A Monte Carlo simulation study

Special Collection: [Monte Carlo methods, 70 years after Metropolis et al. \(1953\)](#)

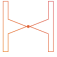
Parsa Habibi ; Poulumi Dey ; Thijs J. H. Vlugt ; Othonas A. Moulτος  


 Check for updates


J. Chem. Phys. 161, 054304 (2024)


<https://doi.org/10.1063/5.0221004>




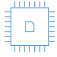
 Nanotechnology & Materials Science


 Optics & Photonics

 Impedance Analysis

 Scanning Probe Microscopy

 Sensors


 Failure Analysis & Semiconductors



Unlock the Full Spectrum. From DC to 8.5 GHz.

Your Application. Measured.

[Find out more](#)



Effect of dissolved KOH and NaCl on the solubility of water in hydrogen: A Monte Carlo simulation study

Cite as: J. Chem. Phys. 161, 054304 (2024); doi: 10.1063/5.0221004

Submitted: 29 May 2024 • Accepted: 15 July 2024 •

Published Online: 1 August 2024







View Online



Export Citation



CrossMark

Parsa Habibi,^{1,2}  Poulumi Dey,²  Thijs J. H. Vlugt,¹  and Othonas A. Moutos^{1,a)} 

AFFILIATIONS

¹ Engineering Thermodynamics, Process and Energy Department, Faculty of Mechanical Engineering, Delft University of Technology, Leeghwaterstraat 39, 2628 CB Delft, The Netherlands

² Department of Materials Science and Engineering, Faculty of Mechanical Engineering, Delft University of Technology, Mekelweg 2, 2628 CD Delft, The Netherlands

Note: This paper is part of the JCP Special Topic on Monte Carlo Methods, 70 Years After Metropolis *et al.* (1953).

a) Author to whom correspondence should be addressed: o.moutos@tudelft.nl

ABSTRACT

Vapor–Liquid Equilibria (VLE) of hydrogen (H₂) and aqueous electrolyte (KOH and NaCl) solutions are central to numerous industrial applications such as alkaline electrolysis and underground hydrogen storage. Continuous fractional component Monte Carlo simulations are performed to compute the VLE of H₂ and aqueous electrolyte solutions at 298–423 K, 10–400 bar, 0–8 mol KOH/kg water, and 0–6 mol NaCl/kg water. The densities and activities of water in aqueous KOH and NaCl solutions are accurately modeled (within 2% deviation from experiments) using the non-polarizable Madrid-2019 Na⁺/Cl⁻ ion force fields for NaCl and the Madrid-Transport K⁺ and Delft Force Field of OH⁻ for KOH, combined with the TIP4P/2005 water force field. A free energy correction (independent of pressure, salt type, and salt molality) is applied to the computed infinite dilution excess chemical potentials of H₂ and water, resulting in accurate predictions (within 5% of experiments) for the solubilities of H₂ in water and the saturated vapor pressures of water for a temperature range of 298–363 K. The compositions of water and H₂ are computed using an iterative scheme from the liquid phase excess chemical potentials and densities, in which the gas phase fugacities are computed using the GERG-2008 equation of state. For the first time, the VLE of H₂ and aqueous KOH/NaCl systems are accurately captured with respect to experiments (i.e., for both the liquid and gas phase compositions) without compromising the liquid phase properties or performing any refitting of force fields.

© 2024 Author(s). All article content, except where otherwise noted, is licensed under a Creative Commons Attribution-NonCommercial 4.0 International (CC BY-NC) license (<https://creativecommons.org/licenses/by-nc/4.0/>) <https://doi.org/10.1063/5.0221004>

I. INTRODUCTION

The accurate prediction of Vapor–Liquid Equilibria (VLE) of H₂ and aqueous electrolyte systems (e.g., aqueous NaCl and KOH solutions) is crucial for the design and optimization of environmental and industrial processes such as water electrolysis,^{1–4} electrochemical compression of water,^{5,6} and underground hydrogen storage.^{7–9} For example, the VLE of H₂ and aqueous KOH solutions influences the product gas purities in alkaline water electrolyzers,^{3,10,11} and the presence of water in compressed hydrogen affects the thermophysical properties (e.g., the Joule–Thompson coefficients) of the gaseous mixture.⁶ Excess water can also block

porous membranes in PEM fuel cells.^{12,13} All of these factors are relevant for the production, storage, and subsequent use of H₂.^{4,6,10,12,13}

The VLE of H₂ and aqueous systems are traditionally measured in experiments.^{14–16} Nevertheless, such experiments at high pressures (up to ~700 bar) are costly and time consuming considering the vast range of conditions of interest [i.e., type of aqueous salts, salt molality (*m*), and temperature].^{3,10,17,18} Alkaline water electrolyzers typically operate at ~360 K, 2–8 mol KOH/kg water, and at pressures of 1–100 bar.^{3,10,17} For underground storage of H₂, H₂ gas is in contact with brine solutions with molalities up to 5 mol NaCl/kg water, pressures up to 300 bar, and

temperatures ranging from 348 to 372 K.¹⁸ As an alternative to experiments, molecular simulation, e.g., Monte Carlo (MC), can be used to compute the VLE of H₂ with aqueous electrolyte solutions (i.e., KOH and NaCl) for a wide range of temperatures, pressures, and salt concentrations.^{19–23}

The accuracy of MC simulations depends on the underlying models (i.e., semi-empirical force fields or *ab initio* simulations), which are used to describe the interactions between different species.^{24,25} Two-body force fields with point charges (non-polarizable) are widely used for computing the VLE of H₂ and aqueous electrolyte systems due to their computational efficiency, small number of parameters, and accuracy in predicting various thermophysical properties of aqueous solutions.^{6,19,20,26} Rahbari *et al.*⁶ computed the VLE of H₂ and pure water systems using MC simulations for a temperature range of 298–423 K and pressures up to 1000 bar. Rahbari *et al.*⁶ showed that the TIP4P/2005²⁷ water force field (which is parameterized based on liquid densities, transport properties, and the temperature of maximum density) can accurately model the solubilities of H₂ in water but fails to predict the water content in compressed H₂ gas due to incorrect predictions of the saturated vapor pressure of water. Other non-polarizable water force fields such as TIP3P (which is trained on the vaporization energy of water),^{28,29} do not predict the solubilities of H₂ in water but correctly capture the water content in H₂ gas.⁶ TIP4P/2005 and TIP3P also cannot correctly predict the second virial coefficient (and hence the non-idealities) of water in the gas phase.^{30,31} In other molecular simulation studies in the literature (such as in Refs. 19–22, 32, and 33), the solubilities of H₂ in the aqueous phase are calculated without computing the solubility of water in compressed H₂. This is done by either assuming an ideal H₂ gas phase (for pressures below 100 bar) and computing the Henry constants of H₂ or by neglecting the water content in the gas phase at higher pressures (as the experimental water content is below 1% for temperatures below 363 K and pressures above 100 bar).^{6,19–22,32,33}

Accurate modeling of the free energies in the aqueous solution is necessary for predicting the VLE of H₂ and aqueous electrolyte solutions.²⁶ Non-polarizable force fields of water such as SPC/E³⁴ and TIP4P/2005,²⁷ which accurately model the liquid densities and transport properties,²⁶ cannot accurately predict the free energies of liquid water. Already in 1987, Berendsen *et al.*³⁴ discovered a fundamental issue when parameterizing the non-polarizable SPC/E force field of water, i.e., fitting force fields to the vaporization energies of water results in excluding the self-polarization energy of water (i.e., the “missing term” mentioned in the title of the paper by Berendsen *et al.*³⁴). Berendsen *et al.*³⁴ showed that the inclusion of the self-polarization energy of liquid water by enhancing the dipole moment of water significantly improves predictions of transport properties, densities, and RDFs, at the cost of less accurate predictions for the vaporization energy of water. Recently, we developed a new approach to accurately modeling the free energies of water using the non-polarizable TIP4P/2005 water force field by adding a temperature dependent free energy correction to the partition function of the isolated water molecule.²⁶ The free energy correction is independent of pressure, salt type, and molality and leads to accurate predictions for saturated vapor pressures in water. This free energy correction can be used to correct for the influence of the self-polarization energy (i.e., the “missing term”) on the computed free energies and is especially rel-

evant for systems that exhibit strong electrostatic interactions and polarizability.²⁶

Despite the importance of the VLE data for H₂ and aqueous electrolyte (i.e., KOH and NaCl) solutions, none of the existing molecular simulation studies have accurately computed both the equilibrium water composition in H₂ and the solubilities of H₂ in aqueous solutions at different KOH and NaCl concentrations. In this work, the excess chemical potentials (i.e., with respect to the ideal gas reference state³⁵) of H₂ and water in the liquid phase are computed using Continuous Fractional Component Monte Carlo (CFCMC)^{35–37} simulations. As derived in Ref. 26, a temperature-dependent free energy correction is used to shift the excess chemical potential of the TIP4P/2005 water force field (at a molality of 0 mol salt/kg water). A constant free energy correction for the infinite dilution excess chemical potential of the Marx H₂ force field³⁸ in TIP4P/2005²⁷ is also applied. This results in an accurate prediction of H₂ solubilities in water (and the temperature of minimum H₂ solubility in water) for 298–363 K at a H₂ fugacity of 1 bar (within 5% deviation from experiments¹⁵). The Madrid-Transport K⁺³⁹ and the Delft Force Field of OH⁻ (DFF/OH⁻)²⁰ are used to model KOH, and the Madrid-2019 force fields⁴⁰ of Na⁺ and Cl⁻ are used to model NaCl. These ion force fields are shown to accurately model the densities and activities of water (and their temperature-dependence) with respect to experiments (within 2% deviation). The equilibrium compositions of H₂ and water are computed from the liquid phase excess chemical potentials and densities using an iterative scheme in which the gas phase fugacities and densities are computed using the GERG-2008 Equation of State (EoS).⁴¹ This approach accurately predicts the scarcely available experimental equilibrium compositions of water and H₂ for H₂/aqueous NaCl systems^{14,15} (within 5%) without any refitting of force fields or modifying the Lorentz–Berthelot²⁴ (LB) mixing rules. The CFCMC simulations are then performed for a wide range of conditions to simulate the VLE of H₂ and aqueous electrolyte solutions at 298–423 K, 10–400 bar, 0–8 mol KOH/kg water, and 0–6 mol NaCl/kg water.

This paper is organized as follows. In Sec. II, details are provided for force fields, the CFCMC simulations, the free energy correction, and the iterative scheme for computing the VLE of H₂ and aqueous KOH/NaCl solutions. In Sec. III, the computed densities and activities of water (and their temperature dependence) for aqueous KOH and NaCl solutions are shown, the influence of the free energy correction on the saturated vapor pressure of water and solubility of H₂ in pure water is discussed, and the VLE data for H₂ and aqueous KOH and NaCl solutions are provided. Conclusions and recommendations are outlined in Sec. IV.

II. COMPUTATIONAL METHODS

A. Force fields

Water is modeled using the four-site rigid TIP4P/2005²⁷ force field. For aqueous NaCl solutions, the Na⁺ and Cl⁻ force fields of Madrid-2019⁴⁰ are used. For aqueous KOH solutions, the K⁺ ions are modeled using the Madrid-Transport force field,³⁹ and the OH⁻ ions are modeled using the Delft Force Field of OH⁻ (DFF/OH⁻).²⁰ H₂ is modeled using the three-site Marx³⁸ force field. The combination of Marx³⁸ H₂ and TIP4P/2005 water has performed accurately in prior studies in predicting the diffusivities and solubilities of H₂

in water.^{19,20,22,33,42} The force field choices are justified in Sec. III of this work. Ion charges are commonly scaled in non-polarizable models.^{39,40,43} In Madrid-2019,⁴⁰ the unit charge of ions is scaled by a factor of 0.85, and in Madrid-Transport³⁹ and DFF/OH⁻,²⁰ charges are scaled by a factor of 0.75. Charge scaling leads to accurate density, viscosity, electrical conductivities, and water activity predictions for aqueous electrolyte solutions (e.g., NaCl and KOH) compared to using unscaled charges.^{19,20,33,40,44} Charge scaling is discussed in detail in Refs. 39, 40, and 45. All force field parameters for H₂O, Na⁺, Cl⁻, K⁺, OH⁻, and H₂ are listed in Tables S1–S5 of the [supplementary material](#). The LB mixing rules^{24,25} are used in all simulations, with the exception of [Na⁺/K⁺/Cl⁻-H₂O] and [Na⁺-Cl⁻] Lennard-Jones (LJ) interactions as specified in Tables S3 and S4 of the [supplementary material](#). The Ewald summation²⁴ is used for electrostatic interactions (relative precision of 10⁻⁶). A cutoff radius of 10 Å is used for the LJ interactions and the real space contribution of the Ewald-Summation, as the Madrid-2019⁴⁰ Na⁺/Cl⁻, the Madrid-Transport³⁹ K⁺, and the DFF/OH⁻ force fields²⁰ are parameterized with this cutoff radius. Analytic tail corrections for energies and pressures are applied for the LJ part of the interactions.

B. MC simulations

A schematic of our computational methodology is shown in [Fig. 1](#). To compute the VLE of H₂ and aqueous electrolyte solutions of NaCl and KOH, the chemical potentials of H₂O and H₂ in the liquid phase are equated to the gas phase chemical potentials at constants T and P . The liquid phase chemical potentials are computed using CFCMC simulations,^{35–37} which are carried out using the open-source BRICK-CFCMC software package^{46,47} in the Continuous Fractional Component isobaric-isothermal (CFCNPT) ensemble.^{35–37} The gas phase is modeled using the GERG-2008 EoS,⁴¹ as the TIP4P/2005 water force field is a poor EoS of water in the vapor phase.³⁰ For all CFCNPT simulations, periodic boundary conditions are applied in all directions of the cubic simulation box. The simulations consist of 300 water molecules and 0–43 molecules of KOH (corresponding to 0–8 mol KOH/kg water) or 0–32 molecules of NaCl (corresponding to 0–6 mol NaCl/kg water), depending on the molalities of the solution. The exact numbers of KOH and NaCl molecules and the corresponding molalities are provided in Tables S6 and S7 of the [supplementary material](#). The VLE of H₂ and aqueous NaCl/KOH solutions are calculated at the following temperatures: 298, 323, 363, 393, and 423 K. The pressures considered are 10, 50, 100, 200, and 500 bar.

To compute the chemical potentials of H₂O and H₂, the excess chemical potentials of H₂ and H₂O (i.e., with respect to the ideal gas reference state³⁵) in the aqueous phase are required. The excess chemical potentials of H₂ and H₂O are computed by introducing a single fractional molecule of H₂ and H₂O. For details on the fractional molecules, the λ parameter (an order parameter that modifies the interactions of fractional molecules with surrounding molecules), and the sampling of the λ -space in CFCMC simulations, the reader is referred to Refs. 35–37 and 46. At $\lambda = 0$, fractional molecules behave as an ideal gas molecule, and at $\lambda = 1$, the fractional molecules fully interact with the surrounding molecules. The probability of occurrence for different λ values is computed by

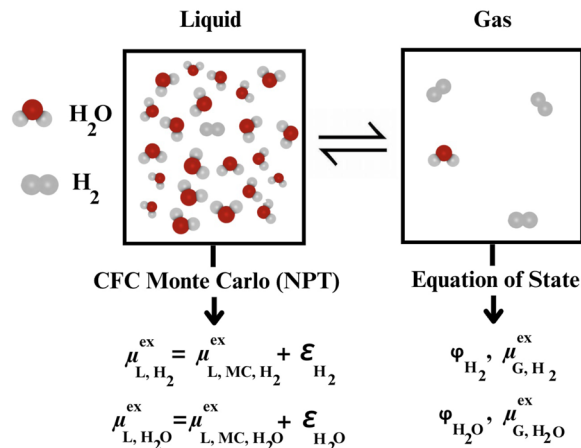


FIG. 1. Schematic representation of the methodology used in this work. To compute the vapor–liquid equilibrium (VLE) of H₂ and aqueous electrolyte (i.e., KOH and NaCl) systems, the chemical potentials of water and H₂ in the liquid phase are equated with the gas phase chemical potentials at constant temperature and pressure. Continuous fractional component Monte Carlo (CFCMC)^{35–37} simulations are used to compute the excess chemical potentials ($\mu_{L,MC,i}^{\text{ex}}$ for species i) of water and H₂ in the liquid phase. These excess chemical potentials are then shifted using the free energy correction, ϵ_i , [as described in Ref. 26 and Eq. (3) in this manuscript], to yield the final $\mu_{L,i}^{\text{ex}}$. The compositions of water and H₂ are computed using an iterative scheme as discussed in Sec. II, in which the gas phase excess chemical potentials ($\mu_{G,i}^{\text{ex}}$) and fugacity coefficients (ϕ_i) are obtained from the GERG-2008 equation of state.⁴¹

constructing a histogram of 100 bins. The Wang–Landau algorithm^{48,49} is used to create a biasing function for λ [$W(\lambda)$] to avoid sampling issues due to energy barriers in λ -space (i.e., to create a flat observed probability distribution in λ -space). The Boltzmann probability distribution of λ [$p_B(\lambda)$] is then computed using the observed probability distributions of λ [$p_{\text{obs}}(\lambda)$] and $W(\lambda)$ using^{19,20,35}

$$p_B(\lambda) = \frac{\langle p_{\text{obs}}(\lambda) \exp[-W(\lambda)] \rangle}{\langle \exp[-W(\lambda)] \rangle}, \quad (1)$$

in which the brackets indicate ensemble averages. The liquid phase excess chemical potentials of species i ($\mu_{L,MC,i}^{\text{ex}}$) are computed using^{19,20,35}

$$\mu_{L,MC,i}^{\text{ex}} = -k_B T \ln \frac{p_B(\lambda = 1)}{p_B(\lambda = 0)}, \quad (2)$$

where $p_B(\lambda = 1)$ and $p_B(\lambda = 0)$ are the Boltzmann probabilities of λ for $\lambda = 1$ and $\lambda = 0$, respectively.^{19,20,35} The computed excess chemical potentials of water and H₂ at a salt molality of 0 mol salt/kg water are corrected using a free energy correction ϵ_i . Details on this free energy correction are given in Ref. 26. The TIP4P/2005 force field can accurately model the change in free energy as a function of pressure or salt molality, but not the absolute values of the excess chemical potentials.²⁶ To correct for the initial offset of the excess

chemical potentials of water and H₂ at $m = 0$, the computed excess chemicals are shifted using

$$\mu_{L,i}^{\text{ex}} = \mu_{L,MC,i}^{\text{ex}} + \epsilon_i, \quad (3)$$

where $\mu_{L,i}^{\text{ex}}$ refers to the corrected excess chemical potential of species i in the liquid phase. The free energy correction for TIP4P/2005²⁷ ($\epsilon_{\text{H}_2\text{O}}$) is derived in Ref. 26 and is a weak function of temperature,

$$\epsilon_{\text{H}_2\text{O}} = A_0 + A_1 T, \quad (4)$$

where $A_0 = 5.00 \text{ kJ mol}^{-1}$ and $A_1 = -4.36 \times 10^{-3} \text{ kJ mol}^{-1} \text{ K}^{-1}$. A_0 and A_1 are fitted parameters (i.e., for TIP4P/2005²⁷) and differ for different water force fields.²⁶ Using the free energy correction term $\epsilon_{\text{H}_2\text{O}}$, the computed excess chemical potentials of water in the liquid phase using the TIP4P/2005²⁷ force field match the experimental values.²⁶ The free energy correction for the infinite dilution excess chemical potential of Marx H₂ (ϵ_{H_2}) in TIP4P/2005 water is independent of temperature and is equal to $\epsilon_{\text{H}_2} = -0.27 \text{ kJ mol}^{-1}$ (computed in this work based on the solubilities of H₂ in water at 298 K and a H₂ fugacity of 1 bar).

Equating the chemical potential of water in the liquid phase with the gas phase results in Ref. 26,

$$y_{\text{H}_2\text{O}} = \frac{k_B T \rho_{L,\text{H}_2\text{O}}}{P \phi_{\text{H}_2\text{O}}} \exp \left[\frac{\mu_{L,\text{H}_2\text{O}}^{\text{ex}}}{k_B T} \right], \quad (5)$$

where $y_{\text{H}_2\text{O}}$ is the gas phase mole fraction of water, $\phi_{\text{H}_2\text{O}}$ is the fugacity coefficient of water, and $\rho_{L,\text{H}_2\text{O}}$ is the number density of water in the liquid phase (in units of molecules/m³). Equation (5) is derived from the [supplementary material](#) in Ref. 26. Here, the gas phase consists of only H₂ and H₂O (i.e., $y_{\text{H}_2} + y_{\text{H}_2\text{O}} = 1$) since salts such as NaCl and KOH are not volatile. $y_{\text{H}_2\text{O}}$, y_{H_2} , and ρ_{L,H_2} (i.e., solubility of H₂ in the liquid phase) are unknowns. Equation (5) is solved iteratively by initially assuming that $\phi_{\text{H}_2\text{O}} = 1$. Starting from an initial value of $y_{\text{H}_2\text{O}}$ (and y_{H_2} as we have a binary gas mixture), the value of $\phi_{\text{H}_2\text{O}}$ is updated at the given composition, T , and P using the GERG-2008 EoS.⁴¹ The new value of $\phi_{\text{H}_2\text{O}}$ is then used to update $y_{\text{H}_2\text{O}}$. This is repeated until $y_{\text{H}_2\text{O}}$ is changed by less than 0.1%. The non-ideality of gaseous H₂-H₂O mixtures is captured using GERG-2008 EoS⁴¹ instead of using the TIP4P/2005 water and Marx H₂ force fields, as TIP4P/2005 cannot accurately model the virial coefficients of gaseous water^{30,50} and hence neither the non-idealities of the gas phase. After obtaining $y_{\text{H}_2\text{O}}$ and y_{H_2} , the number density of H₂ in the liquid phase ρ_{L,H_2} can be computed using

$$\rho_{L,\text{H}_2} = \frac{P \phi_{\text{H}_2} y_{\text{H}_2}}{k_B T} \exp \left[-\frac{\mu_{L,\text{H}_2}^{\text{ex}}}{k_B T} \right]. \quad (6)$$

Equation (6) is a rearrangement of Eq. (5) for H₂. Equation (6) assumes that the excess chemical potential of H₂ in the liquid phase $\mu_{L,\text{H}_2}^{\text{ex}}$ is independent of the H₂ density in the aqueous phase, i.e., that $\mu_{L,\text{H}_2}^{\text{ex}}$ is equal to the infinite dilution excess chemical potential, computed using a single fractional molecule of H₂ plus the correction term ϵ_{H_2} . This assumption is valid, as the mole fraction (i.e., solubility) of H₂ in the aqueous phase is well below 1% for all the

conditions considered in this work.⁶ ρ_{L,H_2} is converted to the unit of mole fraction in the aqueous phase using

$$x_{\text{H}_2} = \frac{\rho_{L,\text{H}_2} \langle V \rangle}{n_{\text{H}_2\text{O}} + n_s + \rho_{L,\text{H}_2} \langle V \rangle}, \quad (7)$$

where $\langle V \rangle$ is the ensemble averaged volume of the simulation box, computed in the CFCNPT ensemble. $n_{\text{H}_2\text{O}}$ and n_s are the number of moles of H₂O and salt (i.e., NaCl or KOH) in the simulation box, respectively. The activity coefficient of H₂O ($\gamma_{\text{H}_2\text{O}}$) in the liquid phase at a molality m of salt can be computed using the excess chemical potential of pure water ($\mu_{\text{H}_2\text{O},0}^{\text{ex}}$) and in solution ($\mu_{\text{H}_2\text{O},m}^{\text{ex}}$) according to Ref. 51,

$$\gamma_{\text{H}_2\text{O}} = \frac{\rho_{L,\text{H}_2\text{O},m}}{x_w \rho_{L,\text{H}_2\text{O},0}} \exp \left[\frac{\mu_{\text{H}_2\text{O},m}^{\text{ex}} - \mu_{\text{H}_2\text{O},0}^{\text{ex}}}{k_B T} \right], \quad (8)$$

where $\rho_{L,\text{H}_2\text{O},m}$ and $\rho_{L,\text{H}_2\text{O},0}$ are the number density of water molecules in a solution with salt of molality m and in the pure water solution, respectively. $x_{\text{H}_2\text{O}}$ is the mole fraction of water in the aqueous solution. The activity of water ($a_{\text{H}_2\text{O}}$) can be computed by multiplying the activity coefficient and mole fraction of water in the liquid phase, i.e., $a_{\text{H}_2\text{O}} = \gamma_{\text{H}_2\text{O}} \times x_{\text{H}_2\text{O}}$.

In all simulations, 2×10^5 equilibration cycles are carried out, followed by 1×10^6 production cycles. A cycle refers to N trial moves, with N corresponding to the total number of molecules, with a minimum of 20. Trial moves are selected with the following probabilities: 29% rotations, 35% translations, 1% volume changes, 25% λ changes, and 10% reinsertions of fractional molecules at random locations inside the simulation box. The maximum displacements for volume changes, molecule translations, rotations, and λ changes are adjusted to obtain an acceptance probability of ~50%. For a detailed discussion of the CFCMC simulations, the reader is referred to Refs. 46 and 47. For each pressure, temperature, and salt concentration, 100 independent simulations are performed. The Boltzmann probability distributions are averaged from blocks of 20 simulations to obtain 5 independent distributions for the order parameter λ of water and H₂, from which the uncertainties are computed. For all averaged distributions, the excess chemical potentials, activities of water, and solubilities of H₂ are calculated to obtain a mean value and the standard deviation of the 5 independent blocks. All raw data are listed in Tables S8-S13 of the [supplementary material](#).

III. RESULTS AND DISCUSSION

A. Liquid phase densities and activities of water

Before computing the VLE of aqueous KOH/NaCl solutions and H₂, the densities and activities of water in the liquid phase are validated with respect to experimental data. [Figures 2\(a\)](#) and [2\(b\)](#) show the liquid densities as functions of the salt molality for aqueous KOH and NaCl solutions, respectively, at 298 and 363 K at 50 bar. The experimental correlations of Laliberté and Cooper⁵² for aqueous NaCl and KOH solutions are used for comparison. These correlations can accurately model the densities of various aqueous salts (e.g., NaCl, KOH, LiCl, and AlCl₃) with average deviations of 0.1 kg m^{-3} compared to experiments. As shown in [Figs. 2\(a\)](#) and [2\(b\)](#), the MC results computed using the Madrid-Transport K⁺,³⁹

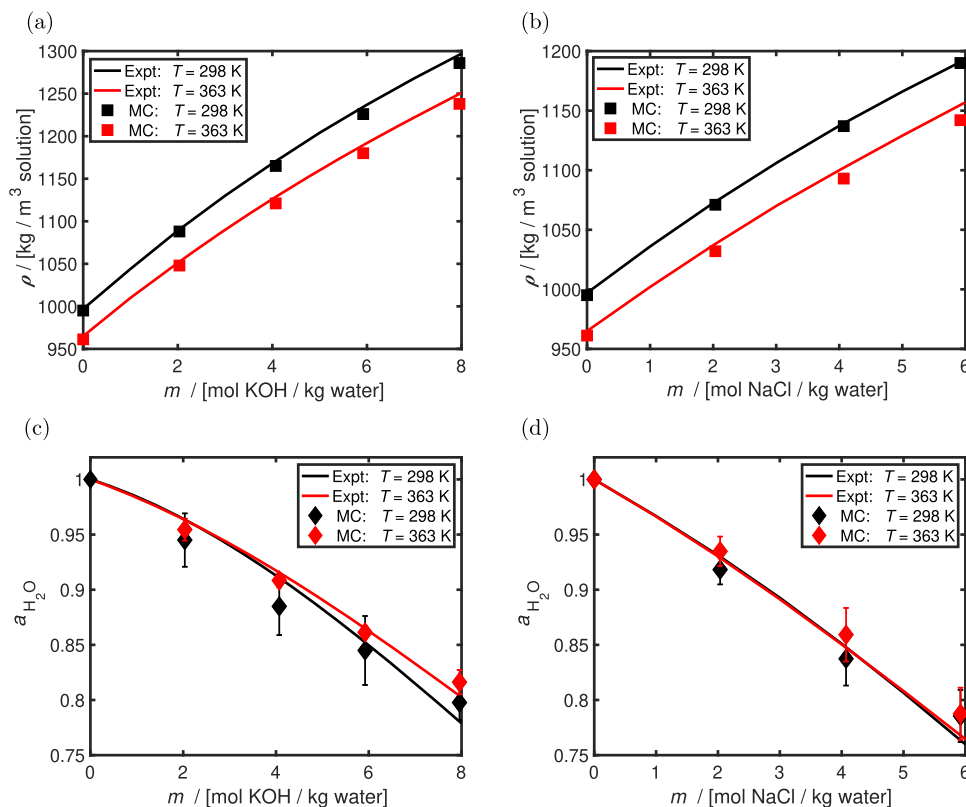


FIG. 2. Computed liquid densities (ρ) in units of kg/m^3 solution for aqueous (a) KOH and (b) NaCl solutions as functions of salt molality (m) in units of mol salt/kg water. Computed activities of water for aqueous (c) KOH and (d) NaCl solutions as functions of m . ρ and $a_{\text{H}_2\text{O}}$ are computed at 298 and 363 K at 50 bar. The experimental correlation of Laliberté and Cooper⁵² for densities of aqueous KOH and NaCl solutions is shown in (a) and (b) at 298 and 363 K as solid lines. The experimental correlation of Balej⁵³ and the data of Clarke and Glew⁵⁴ for $a_{\text{H}_2\text{O}}$ of aqueous KOH and NaCl solutions are used, respectively.

the DFF/OH⁻,²⁰ and Madrid-2019 Na⁺/Cl⁻ force fields⁴⁰ combined with TIP4P/2005²⁷ can accurately model the variations of the liquid density with respect to KOH/NaCl molality and temperature compared to the experimental correlations (deviations smaller than 1%).

Figures 2(c) and 2(d) show the computed activities of water as functions of KOH/NaCl molalities at 298 and 363 K at 50 bar. The experimental correlation of Balej⁵³ and Clarke and Glew⁵⁴ for the activities of aqueous KOH and NaCl solutions is shown as solid lines in Figs. 2(c) and 2(d), respectively. As shown in Fig. 2(c), the activities of aqueous KOH solutions can be computed accurately with respect to experiments (within error bars) using the non-polarizable Madrid-Transport K⁺,³⁹ DFF/OH⁻²⁰ (with scaled charges of +0.75 [e]/-0.75 [e]), and TIP4P/2005 water. To the best of our knowledge, this is the first time that the activities of water in aqueous KOH solutions have been computed using molecular simulations. The experimental activities of water in aqueous KOH solutions show a small temperature dependence (i.e., ~3% deviation between $a_{\text{H}_2\text{O}}$ at 298 K and 363, at 8 mol KOH/kg water). The slight increase of $a_{\text{H}_2\text{O}}$ as a function of temperature is also observed in the MC simulations [Fig. 2(c)], despite the fact that the error bars are of the same order of magnitude as the variations in temperature. As discussed

by Resnik and Chirife⁵⁵ for aqueous NaCl, LiCl, and H₂SO₄ solutions, the temperature dependence of water activities depends on the specific salt type and is mainly present at higher salt concentrations (i.e., up to 4 mol salt/kg water, barely any temperature dependence is experimentally observed).

As shown in Fig. 2(d), the non-polarizable Madrid-2019 Na⁺/Cl⁻ force fields (with scaled charges of +0.85/-0.85 [e]) combined with TIP4P/2005 can accurately capture the experimental activities of water in aqueous NaCl solutions. These results are in line with the findings of Ref. 26. Accurate modeling of the activities of water entails that the change in the chemical potential of water (i.e., $\mu_{\text{H}_2\text{O},m}^{\text{ex}} - \mu_{\text{H}_2\text{O},0}^{\text{ex}}$) and the liquid densities as a function of m are well-captured in the MC simulations. This also ensures that the variation of the water content in the gas phase ($y_{\text{H}_2\text{O}}$) as a function of KOH/NaCl can be correctly predicted.

B. Gas phase fugacity coefficients

Accurate calculations for the VLE of water and H₂ systems require models that can model both the densities and excess chemical potentials of the liquid phase and the fugacity coefficients of the gas phase [as shown in Eq. (5) of the methodology section].

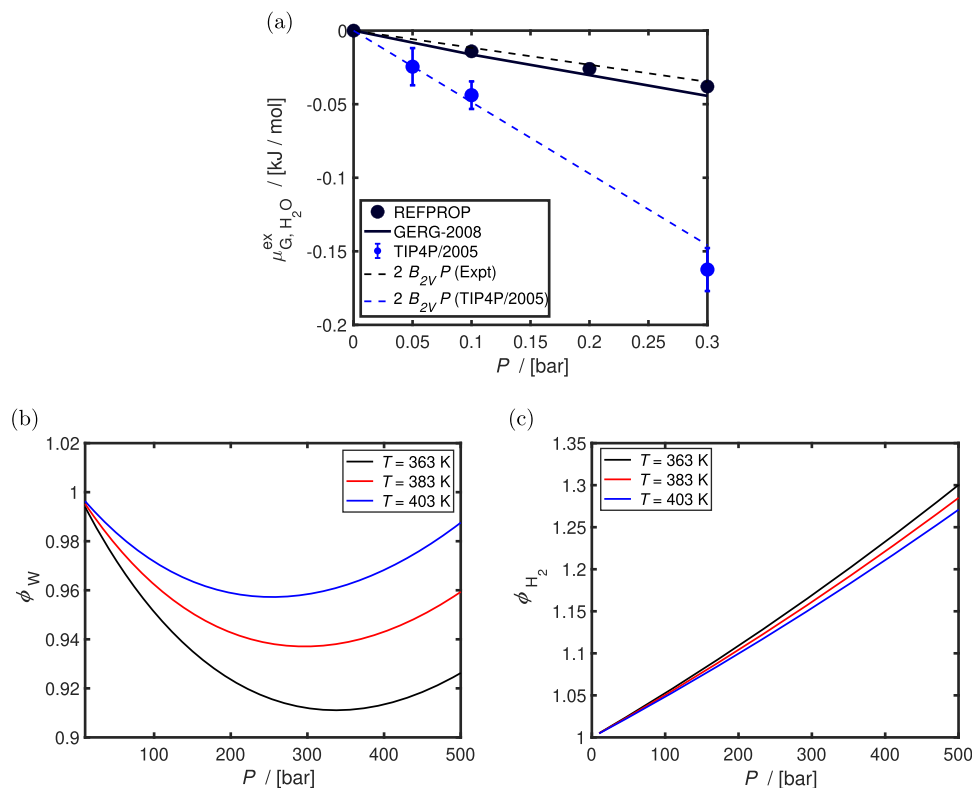


FIG. 3. Computed (a) excess chemical potentials (i.e., μ_{G,H_2O}^{ex} with respect to the ideal gas reference state) of pure gaseous TIP4P/2005 water²⁷ as a function of pressure (P) at 350 K. The computed μ_{G,H_2O}^{ex} values are compared to the data from REFPROP⁵⁶ and the GERG-2008 equation of state⁴¹ for pure water. μ_{G,H_2O}^{ex} can be estimated from the second virial coefficient (B_{2V}) of water vapor (the derivation is shown in Sec. S1 of the [supplementary material](#)). Values of B_{2V} for water vapor (experimental) and TIP4P/2005 at 350 K are obtained from Harvey and Lemmon⁵⁷ and Rouha *et al.*,³⁰ respectively. Computed fugacity coefficients of (b) water (ϕ_{H_2O}) and (c) H₂ (ϕ_{H_2}) in the gas phase as functions of total pressure (P) at 363, 383, and 403 K. The fugacity coefficients are computed at a water mole fraction (y_{H_2O}) of 0.001 and a H₂ mole fraction (y_{H_2}) of 0.999 using the GERG-2008 equation of state.⁴¹

Figure 3(a) shows the computed (using CFCMC simulations) excess chemical potentials of gaseous TIP4P/2005²⁷ (μ_{G,H_2O}^{ex}) at 350 K as a function of P . The MC simulations are compared to data from REFPROP⁵⁶ and the GERG-2008 EoS.⁴¹ μ_{G,H_2O}^{ex} is also approximated using the second virial coefficients of both gaseous water (experimental) and TIP4P/2005 water force fields reported by Harvey and Lemmon⁵⁷ and Rouha *et al.*,³⁰ respectively. The relation between the fugacity coefficient of water, excess chemical potentials of water, and the second virial coefficient is shown in Sec. S1 of the [supplementary material](#). As shown in Fig. 3(a), TIP4P/2005 overestimates the non-ideality of the gas phase (i.e., more negative excess chemical potentials) compared to the data of REFPROP.⁵⁶ The results of Fig. 3(a) show that the TIP4P/2005 force field, which is trained on the liquid phase properties, should not be used to make predictions for the gas phase (e.g., for fugacities and μ_{G,H_2O}^{ex}).

Instead of using classical non-polarizable force fields to model the gas phase, the GERG-2008 EoS⁴¹ is used to model the relation between composition, T , P , ϕ , and the gas phase densities. The GERG-2008 EoS⁴¹ is the ISO-standard for natural gases and

is trained based on 21 natural gases (including H₂ and water vapor) and their binary mixtures. This EoS can model the excess chemical potentials of pure gaseous water with deviations of ~ 0.005 kJ/mol at 350 K and 0.3 bar [shown in Fig. 3(a)]. The computed fugacity coefficients (using the GERG-2008 EoS⁴¹) of water and H₂ as functions of pressure are shown in Figs. 3(b) and 3(c). As shown in Fig. 3, at pressures of already ~ 100 bar, the fugacity coefficients of water and H₂ deviate by more than 5% from ideality in a binary gas mixture with a water mole fraction of 0.001. Simple cubic EoS such as Peng–Robinson⁵⁸ (without optimizing the mixing rules) are not suitable for water and H₂ mixtures due to the polar nature of water, as discussed by Rahbari *et al.*⁶

C. VLE of pure water and solubilities of H₂ in water

In this section, the computed VLE of pure water and the solubilities of H₂ in water are validated against experiments. Figures 4(a) and 4(b) show the computed saturated vapor pressures of water (P_{H_2O}) and solubilities of H₂ (x_{H_2O}) in water, respectively, as functions of temperature. The experimental correlation of Sako *et al.*⁵⁹

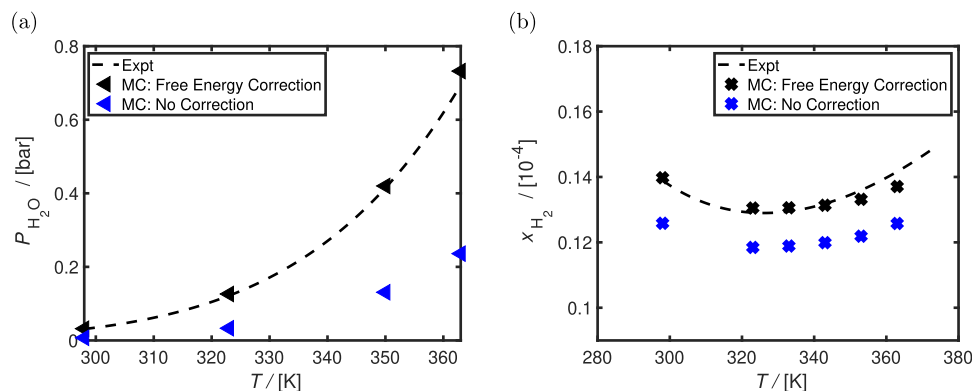


FIG. 4. Computed (a) saturated vapor pressures of pure water ($P_{\text{H}_2\text{O}}$) as a function of temperature T at 1 bar and (b) solubilities of H_2 (x_{H_2}) in units of mole fraction in the liquid phase at a H_2 fugacity of 1 bar. The experimental correlation of Sako *et al.*⁵⁹ is used for the saturated vapor pressures of water, and the correlation of Torin-Ollarves and Trusler¹⁵ is used for the solubilities of H_2 in water. The results computed using the free energy correction [as discussed in Eq. (3) and Ref. 26] for both water and H_2 are compared with the results without the free energy correction.

for the saturated vapor pressure of water and the correlation of Torin-Ollarves and Trusler¹⁵ for the solubilities of H_2 in water are also shown in Figs. 4(a) and 4(b), respectively. The results obtained with and without the free energy correction (as introduced in Eq. (3) and in Ref. 26) are compared in Fig. 4. The free energy correction shifts the excess chemical potentials of water at infinite salt dilution and allows for accurate modeling of the saturated vapor pressures of water using TIP4P/2005.²⁷ Without the free energy correction, the saturated vapor pressures of TIP4P/2005 are underpredicted with respect to the experiments as shown in Fig. 4(a) (i.e., by a factor of 4 at 298 K).

As shown in Fig. 4(b), the solubilities of H_2 in water for a temperature range of 298–363 K can be accurately modeled using the Marx H_2 force field combined with TIP4P/2005²⁷ water, provided that a constant (temperature-independent) free energy correction (trained at 298 K) is applied to the infinite dilution excess chemical potential of H_2 in water. Kerkache *et al.*²² have also accurately modeled the solubilities of H_2 in water using the Marx-TIP4P/2005 combination by modifying the LB²⁴ mixing rules. Kerkache *et al.*²² state that deviating from LB²⁴ mixing rules (by a factor of 1.05) indirectly corrects the influence of polarizability on the free energies, leading to accurate excess chemical potentials of H_2 . The Marx H_2 force field combined with the TIP4P/ μ^5 water force field can accurately model the solubilities of H_2 in water at 298 K, as shown in Fig. S1 of the supplementary material. However, the variation of the H_2 solubilities with respect to temperature is not correctly captured (no minimum in H_2 solubility as observed experimentally¹⁵), resulting in an inaccurate prediction of H_2 solubilities in water at 363 K (by $\sim 20\%$). As shown in this section, applying a free energy correction for H_2 and water is an alternative method to account for polarizability when using non-polarizable force fields, which can lead to an accurate computation of both $P_{\text{H}_2\text{O}}$ and x_{H_2} and their temperature dependence.

D. VLE of aqueous KOH and NaCl solutions and H_2

Figures 5(a) and 5(b) show the computed equilibrium compositions for water vapor ($y_{\text{H}_2\text{O}}$) in H_2 and solubilities of H_2 (x_{H_2}),

respectively, for $\text{H}_2/\text{H}_2\text{O}/\text{salt}$ (i.e., KOH and NaCl) systems at 323 K. At $m = 0$ mol salt/kg water, the experimental data for $y_{\text{H}_2\text{O}}$ in H_2 of Bartlett,¹⁴ which are listed in the supplementary material of Ref. 6, are plotted for comparison. The experimental correlations of Torin-Ollarves and Trusler¹⁵ for x_{H_2} in aqueous NaCl (for $m = 0$ and $m = 6$ mol NaCl/kg water) solutions are shown in Fig. 5(b).

Obtaining both $y_{\text{H}_2\text{O}}$ and x_{H_2} accurately for $\text{H}_2/\text{H}_2\text{O}$ systems using molecular simulations is a difficult endeavor. As discussed by Rahbari *et al.*,⁶ the TIP4P/2005 water force field [without the free energy correction defined in Eq. (3)] cannot accurately capture $y_{\text{H}_2\text{O}}$ because the saturated water vapor pressures are inaccurate, but can capture the experimental values of x_{H_2} . Other water force fields such as TIP3P can accurately predict $y_{\text{H}_2\text{O}}$ and the saturated water vapor pressures but fail to yield precise x_{H_2} because the liquid water interactions are not correctly captured.⁶ For this reason, prior studies^{19,20,32} on molecular simulations of $\text{H}_2/\text{H}_2\text{O}/\text{salt}$ (e.g., NaCl) systems mainly focus on the solubilities of H_2 in the aqueous phase and do not consider the amount of water in the gas phase. Here, both $y_{\text{H}_2\text{O}}$ and x_{H_2} are modeled accurately with respect to the experiments. As shown in Fig. 5(a), the computed $y_{\text{H}_2\text{O}}$ as a function of P shows excellent agreement with the available experimental data at $m = 0$ and 323 K. The computed values of x_{H_2} at $m = 0$ and $m = 6$ mol NaCl/kg water also show excellent agreement with respect to the experimental correlation (within 5% deviations).

As shown in Fig. 5(a), the values for $y_{\text{H}_2\text{O}}$ at $m = 6$ mol NaCl/kg water are quantitatively in line with the values computed at $m = 8$ mol KOH/kg water (both lower by $\sim 20\%$ from the data at $m = 0$). This is consistent with the fact that the activities of water for aqueous KOH at $m = 8$ mol KOH/kg water and for aqueous NaCl at $m = 6$ mol NaCl/kg water are both ~ 0.80 [as shown in Figs. 2(c) and 2(d)]. The solubility of H_2 in the aqueous solution exhibits a stronger decrease as a function of the salt molalities [Fig. 5(b)]. This decrease in H_2 (which is a non-polar gas) solubilities is due to the salting-out effect⁶⁰ and is discussed in Refs. 15, 19, 20, 22, and 61 for aqueous KOH and NaCl solutions.

Figures 5(c) and 5(d) show $y_{\text{H}_2\text{O}}$ as a function of m for aqueous KOH and NaCl solutions, respectively, at 323, 393, and 423 K

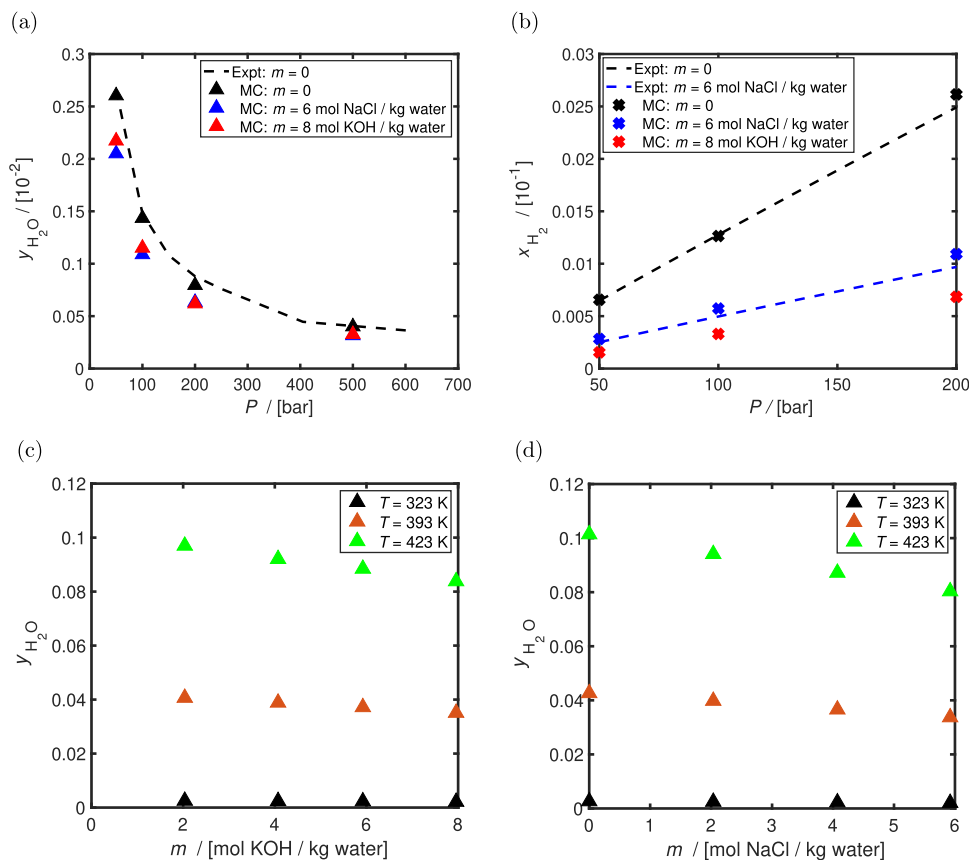


FIG. 5. Computed vapor–liquid equilibrium (VLE) composition of (a) water vapor (y_{H_2O}) in H_2 and (b) H_2 (x_{H_2}) in aqueous NaCl and KOH solutions as functions of pressure at 323 K. The experimental data listed in Ref. 6 at 323 K for y_{H_2O} of pure water (i.e., salt molality of $m = 0$ mol salt/kg water)- H_2 system are also shown (a). The experimental correlation of Torin-Ollarves and Trusler¹⁵ for x_{H_2} in aqueous NaCl solutions is shown in (b) for $m = 0$ and $m = 6$ mol NaCl/kg water. The VLE composition of water vapor in H_2 as functions of m for (c) aqueous KOH and (d) NaCl solutions at 50 bar are shown for 298, 393, and 423 K.

at 50 bar. Temperature has the strongest influence on y_{H_2O} [as discussed in Eq. (5), there is an exponential dependence on $1/T$]. The salt molality changes the computed values of y_{H_2O} by $\sim 10\%$ – 25% for a molality of 4–8 mol salt/kg water, as shown in Fig. 5, with NaCl having a stronger effect on y_{H_2O} values at a given molality compared to KOH. To the best of our knowledge, no other molecular simulation result is available for y_{H_2O} for $H_2/H_2O/salt$ (i.e., KOH and NaCl) systems. The computed y_{H_2O} values for $H_2/H_2O/salt$ systems can be used to model alkaline electrolyzers, electrochemical compression processes, and underground hydrogen storage. All raw data for the computed y_{H_2O} and x_{H_2} values for aqueous KOH/NaCl solutions at 10–500 bar and 298–423 K are shown in Tables S8–S13 of the [supplementary material](#).

IV. CONCLUSIONS

In this work, for the first time, the VLE of H_2 and aqueous KOH/NaCl solutions are computed at 298–423 K, 10–400 bar, 0–8 mol KOH/kg water, and 0–6 mol NaCl/kg water using molecular simulations. The excess chemical potentials of water and H_2 are

computed using CFCMC simulations. Free energy corrections are applied to the computed excess chemical potentials of water and H_2 to accurately model the experimental saturated vapor pressures of water and solubilities of H_2 in water using the TIP4P/2005 water force field and the Marx H_2 force field. Applying a constant free energy correction to the excess chemical potentials of Marx H_2 in TIP4P/2005 water (at a salt molality of 0) results in accurate predictions for H_2 solubilities for a temperature range of 298–373 K. The densities and activities of water (and their temperature dependence) in the aqueous phase for aqueous KOH and NaCl solutions are modeled accurately using the non-polarizable Madrid-2019 force field of Na^+/Cl^- , the Madrid-Transport force field of K^+ , and the DFF/ OH^- force field combined with TIP4P/2005 water (2% deviation with respect to experimental densities and water activities). The compositions of water and H_2 are computed using an iterative scheme from the liquid phase excess chemical potentials and densities, in which the gas phase fugacities are computed using the GERG-2008 EoS. For the first time, the equilibrium compositions of both water and H_2 (and their pressure dependence) for systems of H_2 and aqueous KOH/NaCl solutions are modeled with excellent

agreement with respect to the available experimental data (within 5%) without any additional refitting of force fields or changing the LB mixing rules. The VLE data provided in this work can be used to model the water content in the H₂ stream of alkaline electrolyzers (for aqueous KOH solutions) and for underground hydrogen storage (for aqueous NaCl solutions).

SUPPLEMENTARY MATERIAL

Derivation of the relation between the excess chemical potential (i.e., with respect to the ideal gas reference state) and the second virial coefficient in the gas phase (Sec. S1); computed solubilities of the Marx H₂ force field³⁸ in TIP4P/μ water (discussed in the [supplementary material](#) of Ref. 5) force field (Fig. S1); force field parameters (Tables S1–S5); number of molecules used in CFCMC simulations (Tables S6 and S7); raw data tables for the vapor–liquid equilibria of H₂ and aqueous KOH and NaCl solutions (Tables S8–S13).

ACKNOWLEDGMENTS

This work was sponsored by NWO Domain Science for the use of supercomputer facilities. The authors acknowledge the use of the computational resources of the DelftBlue supercomputer, provided by the Delft High Performance Computing Center (<https://www.tudelft.nl/dhpc>).

AUTHOR DECLARATIONS

Conflict of Interest

The author has no conflicts to disclose.

Author Contributions

Parsa Habibi: Data curation (equal); Formal analysis (equal); Investigation (equal); Methodology (equal); Software (equal); Validation (equal); Visualization (equal); Writing – original draft (equal); Writing – review & editing (equal). **Poulumi Dey:** Data curation (equal); Formal analysis (equal); Funding acquisition (equal); Project administration (equal); Supervision (equal); Writing – review & editing (equal). **Thijs J. H. Vlugt:** Conceptualization (equal); Methodology (equal); Resources (equal); Software (equal); Supervision (equal); Writing – original draft (equal); Writing – review & editing (equal). **Othonas A. Moulτος:** Conceptualization (equal); Funding acquisition (equal); Methodology (equal); Project administration (equal); Resources (equal); Supervision (equal); Writing – original draft (equal); Writing – review & editing (equal).

DATA AVAILABILITY

The data that supports the findings of this study are available within the article and its [supplementary material](#).

REFERENCES

- M. Bodner, A. Hofer, and V. Hacker, *WIREs Energy Environ.* **4**, 365 (2015).
- M. David, C. Ocampo-Martínez, and R. Sánchez-Peña, *J. Energy Storage* **23**, 392 (2019).
- P. Haug, M. Koj, and T. Turek, *Int. J. Hydrogen Energy* **42**, 9406 (2017).
- P. Haug, B. Kreitz, M. Koj, and T. Turek, *Int. J. Hydrogen Energy* **42**, 15689 (2017).
- A. Rahbari, J. C. Garcia-Navarro, M. Ramdin, L. J. P. van den Broeke, O. A. Moulτος, D. Dubbeldam, and T. J. H. Vlugt, *J. Chem. Eng. Data* **66**, 2071 (2021).
- A. Rahbari, J. Brenkman, R. Hens, M. Ramdin, L. J. P. van den Broeke, R. Schoon, R. Henkes, O. A. Moulτος, and T. J. H. Vlugt, *J. Chem. Eng. Data* **64**, 4103 (2019).
- L. Hashemi, M. Blunt, and H. Hajibeygi, *Sci. Rep.* **11**, 8348 (2021).
- B. Pan, X. Yin, Y. Ju, and S. Iglauer, *Adv. Colloid Interface Sci.* **294**, 102473 (2021).
- A. Zarghami, N. Deen, and A. Vreman, *Chem. Eng. Sci.* **227**, 115926 (2020).
- G. Tjarks, J. Mergel, and D. Stolten, “Dynamic operation of electrolyzers—Systems design and operating strategies,” in *Hydrogen Science and Engineering: Materials, Processes, Systems and Technology* (John Wiley & Sons, Ltd, 2016), Chap. XIV, pp. 309–330.
- S. Oikonomidis, M. Ramdin, O. A. Moulτος, A. Bos, T. J. H. Vlugt, and A. Rahbari, *Int. J. Hydrogen Energy* **48**, 34210 (2023).
- W. Schmittinger and A. Vahidi, *J. Power Sources* **180**, 1 (2008).
- X. Wang, Y. Ma, J. Gao, T. Li, G. Jiang, and Z. Sun, *Int. J. Hydrogen Energy* **46**, 12206 (2021).
- E. P. Bartlett, *J. Am. Chem. Soc.* **49**, 65 (1927).
- G. A. Torín-Ollarves and J. M. Trusler, *Fluid Phase Equilib.* **539**, 113025 (2021).
- S. Chabab, P. Théveneau, C. Coquelet, J. Corvisier, and P. Paricaud, *Int. J. Hydrogen Energy* **45**, 32206 (2020).
- J. Hnát, M. Paidar, K. Bouzek, A. Iulianelli, and A. Basile, *Current Trends and Future Developments on (Bio-) Membranes* (Elsevier, Amsterdam, 2020).
- D. Zivar, S. Kumar, and J. Foroozesh, *Int. J. Hydrogen Energy* **46**, 23436 (2021).
- W. A. van Rooijen, P. Habibi, K. Xu, P. Dey, T. J. H. Vlugt, H. Hajibeygi, and O. A. Moulτος, *J. Chem. Eng. Data* **69**, 307 (2024).
- P. Habibi, A. Rahbari, S. Blazquez, C. Vega, P. Dey, T. J. H. Vlugt, and O. A. Moulτος, *J. Phys. Chem. B* **126**, 9376 (2022).
- J. S. Lopez-Echeverry, S. Reif-Acherman, and E. Araujo-Lopez, *Fluid Phase Equilib.* **447**, 39 (2017).
- H. Kerkache, H. Hoang, P. Cézac, G. Galliéro, and S. Chabab, *J. Mol. Liq.* **400**, 124497 (2024).
- C. Vega, J. L. F. Abascal, and I. Nezbeda, *J. Chem. Phys.* **125**, 034503 (2006).
- D. Frenkel and B. Smit, *Understanding Molecular Simulation: From Algorithms to Applications*, 3rd ed. (Elsevier, San Diego, 2023).
- M. Allen, D. Tildesley, and D. Tildesley, *Computer Simulation of Liquids*, 2nd ed. (Oxford Science Publications (Oxford University Press), New York, 2017).
- P. Habibi, H. M. Polat, S. Blazquez, C. Vega, P. Dey, T. J. H. Vlugt, and O. A. Moulτος, *J. Phys. Chem. Lett.* **15**, 4477 (2024).
- J. L. Abascal and C. Vega, *J. Chem. Phys.* **123**, 234505 (2005).
- C. Vega, *Mol. Phys.* **113**, 1145 (2015).
- C. Vega and E. de Miguel, *J. Chem. Phys.* **126**, 154707 (2007).
- M. Rouha, I. Nezbeda, J. Hrubý, and F. Moučka, *J. Mol. Liq.* **270**, 81 (2018).
- K. M. Benjamin, J. K. Singh, A. J. Schultz, and D. A. Kofke, *J. Phys. Chem. B* **111**, 11463 (2007).
- C. Lopez-Lazaro, P. Bachaud, I. Moretti, and N. Ferrando, *BSGF - Earth Sci. Bull.* **190**, 7 (2019).
- P. Habibi, J. R. T. Postma, J. T. Padding, P. Dey, T. J. H. Vlugt, and O. A. Moulτος, *Ind. Eng. Chem. Res.* **62**, 11992 (2023).
- H. J. C. Berendsen, J. R. Grigera, and T. P. Straatsma, *J. Phys. Chem.* **91**, 6269 (1987).
- A. Rahbari, R. Hens, M. Ramdin, O. A. Moulτος, D. Dubbeldam, and T. J. H. Vlugt, *Mol. Simul.* **47**, 804 (2021).
- W. Shi and E. J. Maginn, *J. Chem. Theory Comput.* **3**, 1451 (2007).
- W. Shi and E. J. Maginn, *J. Comput. Chem.* **29**, 2520 (2008).
- D. Marx and P. Nielaba, *Phys. Rev. A* **45**, 8968 (1992).
- S. Blazquez, M. M. Conde, and C. A. Vega, *J. Chem. Phys.* **158**, 054505 (2023).
- I. M. Zeron, J. L. F. Abascal, and C. Vega, *J. Chem. Phys.* **151**, 104501 (2019).
- O. Kunz and W. Wagner, *J. Chem. Eng. Data* **57**, 3032 (2012).
- I. N. Tsimpangogiannis, S. Maity, A. T. Celebi, and O. A. Moulτος, *J. Chem. Eng. Data* **66**, 3244 (2021).

- ⁴³I. V. Leontyev and A. A. Stuchebrukhov, *J. Chem. Theory Comput.* **6**, 1498 (2010).
- ⁴⁴S. Blazquez, J. L. F. Abascal, J. Lagerweij, P. Habibi, P. Dey, T. J. H. Vlugt, O. A. Moulto, and C. Vega, *J. Chem. Theory Comput.* **19**, 5380 (2023).
- ⁴⁵A. Z. Panagiotopoulos, *J. Chem. Phys.* **153**, 010903 (2020).
- ⁴⁶R. Hens, A. Rahbari, S. Caro-Ortiz, N. Dawass, M. Erdős, A. Poursaeidesfahani, H. S. Salehi, A. T. Celebi, M. Ramdin, O. A. Moulto, D. Dubbeldam, and T. J. H. Vlugt, *J. Chem. Inf. Model.* **60**, 2678 (2020).
- ⁴⁷H. M. Polat, H. S. Salehi, R. Hens, D. O. Wasik, A. Rahbari, F. de Meyer, C. Houriez, C. Coquelet, S. Calero, D. Dubbeldam, O. A. Moulto, and T. J. H. Vlugt, *J. Chem. Inf. Model.* **61**, 3752 (2021).
- ⁴⁸F. Wang and D. P. Landau, *Phys. Rev. Lett.* **86**, 2050 (2001).
- ⁴⁹P. Poulain, F. Calvo, R. Antoine, M. Broyer, and P. Dugourd, *Phys. Rev. E* **73**, 056 704 (2006).
- ⁵⁰A. A. Chialvo, A. Bartók, and A. Baranyai, *J. Mol. Liq.* **129**, 120 (2006).
- ⁵¹S. Hempel, J. Fischer, D. Paschek, and G. Sadowski, *Soft Mater.* **10**, 26 (2012).
- ⁵²M. Laliberté and W. E. Cooper, *J. Chem. Eng. Data* **49**, 1141 (2004).
- ⁵³J. Balej, *Int. J. Hydrogen Energy* **10**, 233 (1985).
- ⁵⁴E. C. W. Clarke and D. N. Glew, *J. Phys. Chem. Ref. Data* **14**, 489 (1985).
- ⁵⁵S. L. Resnik and J. Chirife, *J. Food Prot.* **51**, 419 (1988).
- ⁵⁶W. Wagner and A. Pruß, *J. Phys. Chem. Ref. Data* **31**, 387 (2002).
- ⁵⁷A. H. Harvey and E. W. Lemmon, *J. Phys. Chem. Ref. Data* **33**, 369 (2004).
- ⁵⁸D.-Y. Peng and D. B. Robinson, *Ind. Eng. Chem. Fund.* **15**, 59 (1976).
- ⁵⁹T. Sako, T. Hakuta, and H. Yoshitome, *J. Chem. Eng. Data* **30**, 224 (1985).
- ⁶⁰S. Weisenberger and A. Schumpe, *AIChE J.* **42**, 298 (1996).
- ⁶¹S. Shoor, R. D. Walker, Jr., and K. Gubbins, *J. Phys. Chem.* **73**, 312 (1969).